ATLAS
HEC Note-170
13 July 2009

High Rate Effects in the ATLAS HEC Calorimeter

L. Kurchaninov

TRIUMF
4004 Wesbrook Mall, Vancouver, BC, V6T 2A, Canada

Abstract. In this Note I describe a model developed to calculate high rate effects in HEC LAr gaps. The model includes space charge build-up, electron-ion recombination, and voltage drop in HV bias network. Some demonstrative examples are presented for HEC at sLHC and at Protvino beam conditions.

1. Introduction

Theoretical studies of high rate effects in a parallel plate LAr calorimeter in the ATLAS forward region have been performed by John Rutherfoord in year 2000 [1]. With a set of simplifying assumptions a qualitative picture of space charge build-up and signal degradation was obtained. Since that time no attempts have been done (up to my knowledge) to create a model for calculations or simulations of high rate effects in the ATLAS LAr calorimeters.

This Note presents such a model built to study high-rate effects in the HEC. The aim of this model is to predict HEC performance at LHC and sLHC conditions. It will be used first to characterize ionization signals measured in high-intensity beam at IHEP, Protvino, where three mini-modules of LAr end-cap calorimeters are under tests since 2006. These data will be used to adjust uncertain (or unknown) parameters like ion mobility and electron-ion recombination rate constant. The model is built as a numeric solver of equations governing kinetics of electrons and ions in a LAr gap. With minor modifications it can be used for EMC and FCal calorimeters.

In this Note I address only processes of charge build-up in LAr gap and voltage drop in HV line. The calculations of ionization signal shape will be described in a separate Note. I also do not give a detail study of expected HEC performance at the sLHC or Protvino conditions. Such a study will be done later, when the model parameters will be properly tuned. Here I give only a few examples to demonstrate the high-rate effects in LAr gap and to validate model by comparing results of computations with analytical solutions available in some simple cases.

2. Charge kinetics in LAr gap

Consider a gap of width a filled with LAr (dielectric constant $\varepsilon=1.5$) and biased by voltage source V_b through resistor Z. Due to capacitance of gap(s) connected to HV line, a non-zero time constant τ is assumed. In further calculations its value is fixed to 1 *ms*. Ionization in the gap is described by source $J(t)$ (electron-ion pairs per cm^3 per sec.) which is a zero-duration periodic function of time

with period of 25 *ns* in case of LHC and ~1.5 μs for Protvino setup. Due to ionization, some densities of electrons $n_e(t,x)$ and ions $n_i(t,x)$ exist in the gap as a result of balance between pairs generation, recombination and drift. For obvious reasons diffusion is neglected. The kinetic equation for electrons and ions is obvious:

$$\frac{\partial n_e}{\partial t} = J - \frac{\partial}{\partial z}\left(v_e \cdot n_e\right) - R \cdot n_e \cdot n_i$$
$$\frac{\partial n_i}{\partial t} = J + \frac{\partial}{\partial z}\left(v_i \cdot n_i\right) - R \cdot n_e \cdot n_i \qquad (1)$$

Here v_e, v_i, and R are electron drift velocity, ion drift velocity and electron-ion bulk recombination rate. All three values depend on time and coordinate through electric field. Signs in (1) correspond to directions of z-axis and drift velocities shown in Fig.1.

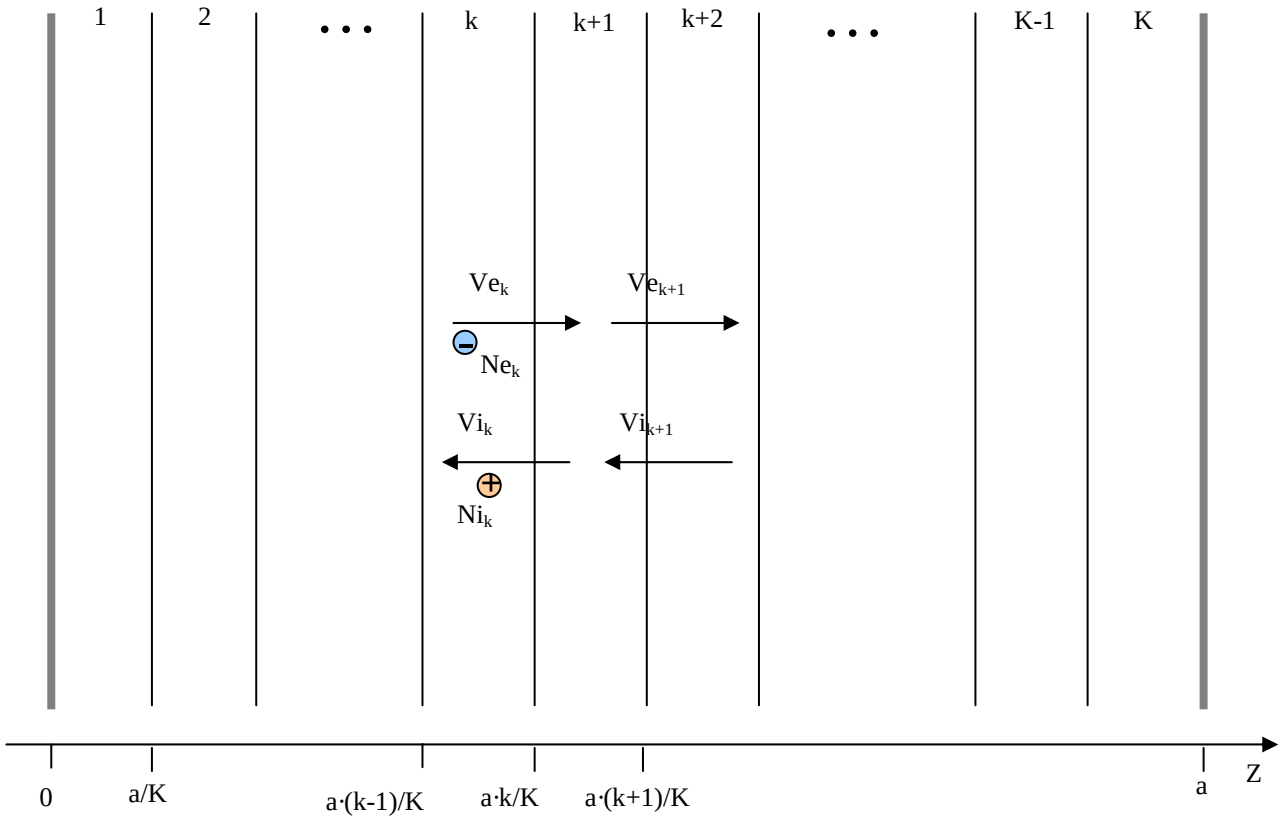

Figure 1*: Electron and ion drift in LAr gap. For numerical calculations the gap is subdivided into K subgaps.*

Presence of space charge changes electric field *E* according to Gauss theorem:

$$\frac{\partial E}{\partial z} = \frac{4 \cdot \pi \cdot q}{\varepsilon} \cdot \left(n_i - n_e\right), \quad \text{or} \quad \frac{\partial^2 V}{\partial z^2} = -\frac{4 \cdot \pi \cdot q}{\varepsilon} \cdot \left(n_i - n_e\right) \qquad (2)$$

where $V(t,z)$ is electric potential fixed at the gap boundaries in the following way:

$$V(t,0)=0, \qquad \text{and} \qquad \tau\cdot\frac{d}{dt}V(t,a)+V(t,a)=V_b-I(t)\cdot Z \tag{3}$$

The last part of eq. (3) describes anode voltage *V(t,a)* which depends on the voltage drop across resistor *Z* and on charging or discharging the anode capacitance. The current *I* in the HV line is a result of drift of charges in all gaps connected to this line. The system (1)-(3) can be solved only for a group of gaps served by the same HV line. In this note I consider the case when HV line is connected to the single gap under study and therefore magnitude of current *I(t)* is solely defined by dynamics of n_e and n_i:

$$I(t)=\frac{q\cdot S}{a}\cdot\int_0^a\left(n_i(t,z)\cdot v_i(t,z)+n_e(t,z)\cdot v_e(t,z)\right)\cdot dz \tag{4}$$

where *S* is the gap area (it is 100 cm^2 in this Note). Eq. (4) is Ramo's expression for current induced by charge moving in the gap.

System (1)-(4) is self-consistent. In some simple cases, considered in sections 4 and 5, it can be solved analytically. In general case it is solvable numerically. The algorithm of computations is straightforward. The gap is subdivided into *K* subgaps as shown in Fig. 1. All functions are considered as constants within each subgap. At initial time *t*=0 first ionization happens and process of drift and recombination is calculated with time step Δt which must be small enough so that electron drift over Δt stays within a small part of the subgap. In further computations, the values of *a*=1.9 *mm*, *K*=80, and Δt=1 *ns* are chosen. For the fastest electron drift velocity, their displacement over Δt is about 16% of the subgap width.

For each time step, functions (actually vectors of *K* numbers) n_e, n_i, v_e, v_i, *E*, and current *I* are recalculated recursively. At *t*=25 ns a new ionization charge is generated and next 25-step cycle of computations repeated. As initial condition, zero values of n_e, n_i and *I* are chosen. This approach gives full description of charge and field distributions in the gap. The solution of equations requires parameterization of ionization yield, drift velocities, and recombination rate vs. electric field strength. The models of these processes are addressed in the next section.

I have to note that in the model described here the actual tracks of ionizing particles are not considered. Both electron and ion densities are uniformly distributed over gap area. In reality a new track can appear very close to one generated previously that will cause significant increase of recombination probability. In other case, the track can be far from all others already existing in the gap and no recombination will happen. In a sense, the approximation of uniform charge distribution provides an average recombination rate, ignoring possible fluctuations. This approximation might be not so bad because each shower contains many ionizing particles and signal is formed by many (16 to 32) gaps.

3. LAr characteristics

Number of electron-ion pairs created by ionization depends on electric field because of the process of initial recombination. There are various models of this process and many publications report results of measurements. Special measurements of ionization yield in HEC have been performed in 2000 run period with one of the serial HEC modules. The results are included in the HEC beam test NIM paper [2], Fig.21. Our data are well approximated by Thomas-Imel model [3] which provides very simple analytical function for probability to escape initial recombination. By using this function, the ionization yield (pairs in gap generated per sec.) reads as:

$$J(E)=\frac{E_v}{W_i\cdot\tau_b\cdot a}\cdot\frac{E}{E_T}\cdot\ln\left(1+\frac{E_T}{E}\right) \tag{5}$$

Here E_v is the energy deposited in the gap per one bunch per unit area (nominal value is 1 *MeV* per 0.19 cm), W_i = 23.6 *eV* – average energy loss spent to create one pair, τ_b – bunch period, E is electric field, and E_T = 0.84 *kV/cm* – parameter of Thomas-Imel model. Eq. (5) is used to calculate source J in (1) for given electric field distribution.

Electron drift velocity in LAr is reported in many papers. One of the HEC measurements is plotted in Fig. 20 of Ref. [2] and reproduced in Fig.2 (points). Our measurements are consistent with majority of others. At the same time there is no complete theory of electron transport in nonpolar liquids. Qualitatively, at low field the drift velocity is proportional to electric field strength and at high fields it saturates due to rise of electrons thermal energy. There is no analytical function offered in literature to describe this dependence. To fit our data I've built an empirical (without any physics behind it) function which is also shown in Fig.2.

$$v_e(E) = v_m \cdot \frac{E}{E_T} \cdot \left(1 + \left(\frac{E}{E_T}\right)^{1/3}\right)^{-3} \qquad (6)$$

It is interesting to note that the field parameter E_T here is exactly the same as in (5). The second parameter is v_m=13.4 *mm/μs*.

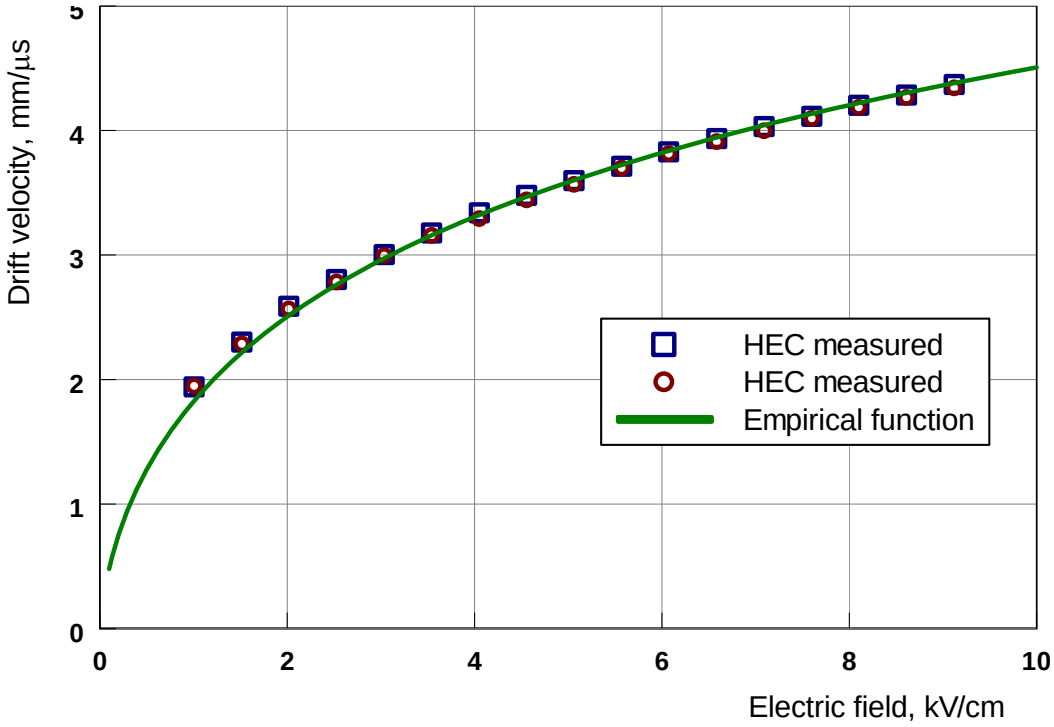

***Figure 2**: Electron drift velocity measured with one of the HEC modules (points) and analytical function (line) used in this Note.*

The positive ion drift has been measured by many groups. All report linear dependence on electric field except of one paper [4] where a step-wise dependence of ion mobility was observed. No reasonable explanation of this dependence was proposed and no other groups observed this effect. Here I assume a constant mobility of ions for full range of electric field:

$$v_i(E) = \mu_i \cdot E \qquad (7)$$

Unfortunately the measured values of mobility reported by different groups vary within an order of magnitude. The value used in this Note is (randomly) chosen as $\mu_i = 6.5 \cdot 10^{-4}$ cm^2/V·s and will be adjusted with Protvino data.

The present knowledge of electron-ion recombination rate is also poor. Perhaps there is only one experimental paper [5] which was published in 1988 and initiated a shower of theoretical investigations. A variety of theories, models and simulation results have been proposed but without any success. Typically all theories give recombination constant 50-100 times less than measured one. Nowadays, (i) results of [5] are not understood and (ii) no other measurements performed with LAr.

Fig. 3 is reproduced from Fig. 8 of Ref. [5] which shows recombination rate constant measured in LAr at 87K. The field range, where these measurements were done is out of our interest. Extrapolation to HEC working point of ~10 kV/cm is impossible; for examples shown below in this Note I use R=10^{-4} cm^3/s that corresponds to the highest field strength plotted in Fig. 3.

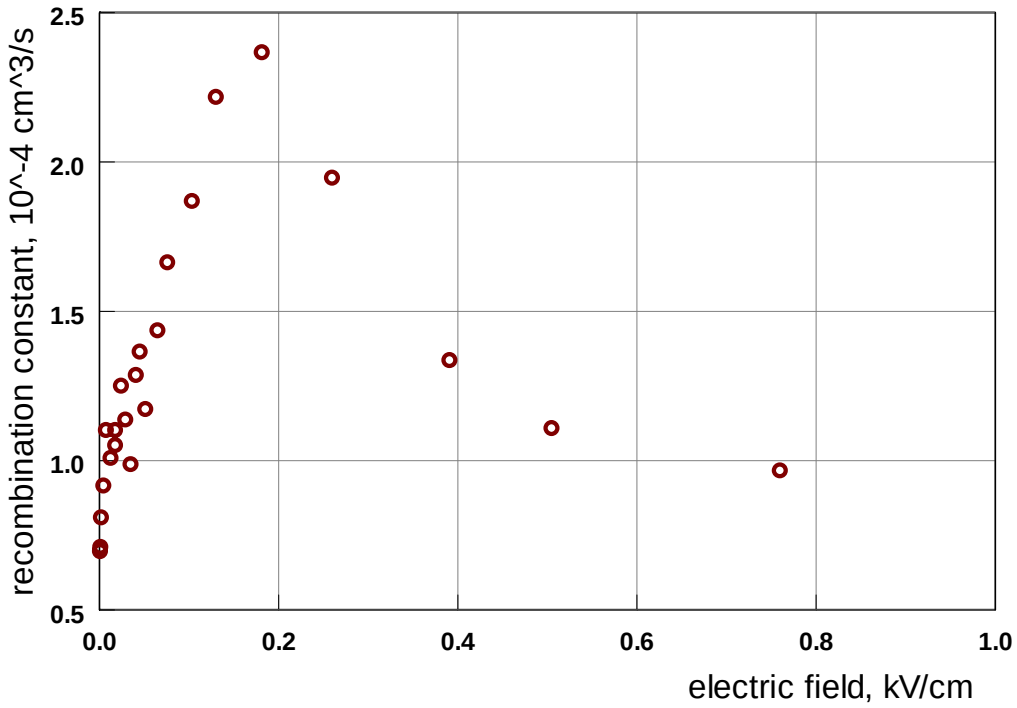

***Figure 3**: Recombination rate constant vs. electric field reproduced from Ref [5].*

Actual value of recombination rate will be (hopefully) adjusted with signal shapes measured at Protvino setup.

The values of various parameters and constants used in subsequent sections are summarized in Appendix. In this Note I refer to those values as “nominal”.

4. Approximation of fast electrons

Electron drift velocity is high and typical drift time through 2-mm gap is about 440 *ns* at E = 10 *kV/cm*. At the same time ions are much slower; typical drift time at this field strength is 30 ms.

Therefore electron space charge builds up much faster. This is demonstrated in Fig. 4 which shows number density (averaged over gap) for electrons and ions within first 2.5 μs of LHC spill. In this initial short time period, recombination and ion drift are negligible as well as voltage drop in HV line. In this simple case (1) reduces to

$$\frac{\partial}{\partial z}\left(v_e \cdot n_e\right) = J; \qquad \frac{\partial n_i}{\partial t} = J$$

with obvious solution

$$n_e(z) = \frac{J}{v_e} \cdot z; \quad \left\langle n_e \right\rangle = \frac{J \cdot a}{2 \cdot v_e}; \quad \text{and} \quad n_i(t) = J \cdot t \tag{8}$$

In the example shown in Fig. 4 (left plot), J=8.55·10^6 $cm^{-3}/\mu s$ and average n_e=1.8·10^6 cm^{-3} that is perfectly reproduced by computational model.

For the time period much shorter than ion drift, the current through gap is due to electrons only. It is approximately constant and equal to $J \cdot q/2$ (times gap volume) and therefore degradation of anode voltage is defined by discharge of gap capacitance:

$$V(t,a) = V_b - I \cdot Z \cdot (1 - \exp(-t/\tau)) \tag{9}$$

Right plot of Fig. 4 shows model computations and eq. (9) for the first half *ms* of the LHC spill. For the conditions of this example current through gap is 13 μA and Z = 1 $M\Omega$.

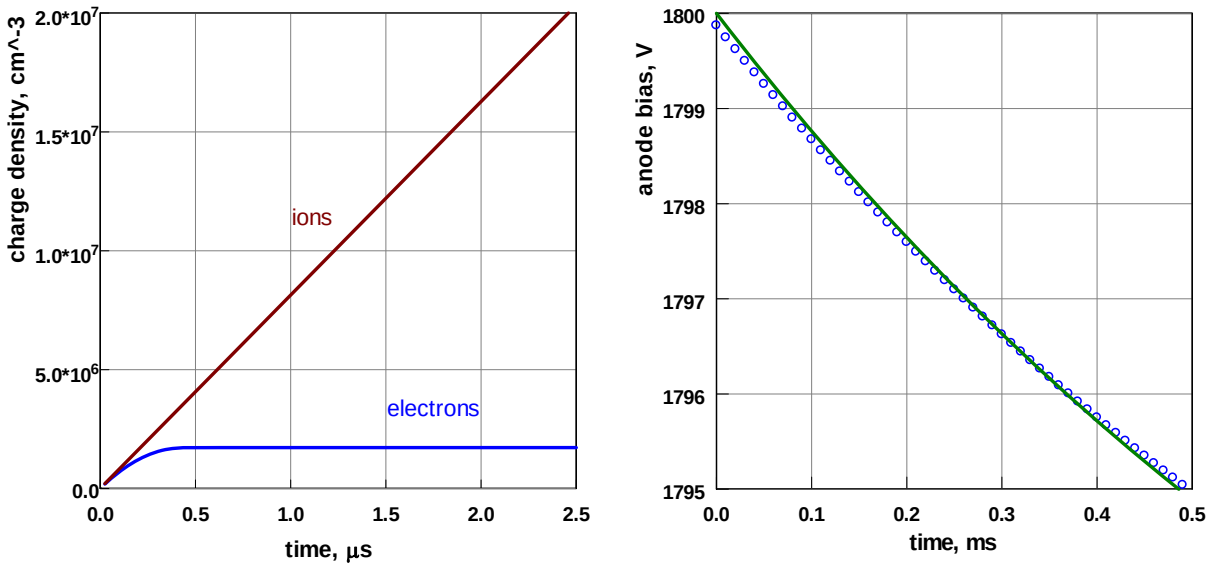

Figure 4*: Charge build-up in the beginning of LHC spill (left) and anode voltage drop due to ionization in gap (right).Points – model computation, line – calculation with (9).*

Since electron drift time is much shorter than both ion drift time and the HV time constant, the numerical calculations can be done with time step much longer than electron drift time (e.g. Δt = 10 μs) so that electron density can be replaced by its stationary value within each time step. In this case (1) read as:

$$\begin{aligned} &\frac{\partial}{\partial z}\left(v_e \cdot n_e\right) + R \cdot n_e \cdot n_i = J \\ &\frac{\partial n_i}{\partial t} = J + \frac{\partial}{\partial z}\left(v_i \cdot n_i\right) - R \cdot n_e \cdot n_i \end{aligned} \tag{10}$$

Now the first equation can be used to calculate $n_e(t,z)$ for given $n_i(t,z)$ and $E(t,z)$, and then increment of n_i for the next time step is calculated with the second equation.

As can be seen from Fig. 4, the electron space charge becomes negligible for the time period longer than few tens of μs and it can be removed from (2). So the field and voltage calculations (2) can also be simplified:

$$\frac{\partial E}{\partial z} = \frac{4 \cdot \pi \cdot q}{\varepsilon} \cdot n_i, \qquad \text{or} \qquad \frac{\partial^2 V}{\partial z^2} = -\frac{4 \cdot \pi \cdot q}{\varepsilon} \cdot n_i \tag{11}$$

The boundary conditions (3) stay the same. Using (11), the field and voltage are calculated for given ion density as follows:

$$\begin{aligned} F_i(z) &= \int_0^z dz' \int_0^{z'} n_i(z'') \cdot dz'' \\ V(z) &= V(a) \cdot \frac{z}{a} + \frac{4 \cdot \pi \cdot q}{\varepsilon} \cdot F_i(a) \cdot \frac{z}{a} - \frac{4 \cdot \pi \cdot q}{\varepsilon} \cdot F_i(z) \\ E(z) &= -\frac{V(a)}{a} - \frac{4 \cdot \pi \cdot q}{\varepsilon} \cdot \frac{F_i(a)}{a} + \frac{4 \cdot \pi \cdot q}{\varepsilon} \cdot F_i'(z) \end{aligned} \tag{12}$$

Comparison of approximate and exact solutions can be seen in Fig. 5. Approximation error stays within 1% for time step between 5 and 20 μs. Computations with approximate equations (10) is 3000 times faster and all further calculations are performed by using this approach with time step of 10 μs.

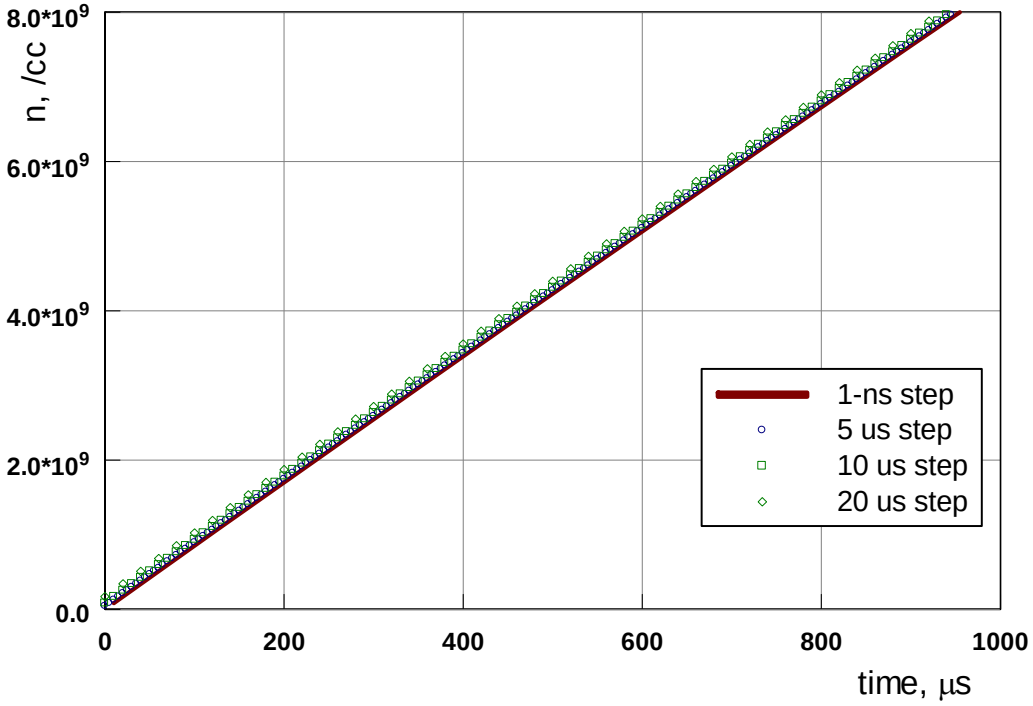

***Figure 5**: Ion build-up calculated with exact equations (1) and with approximation (10) with various time steps.*

5. Analytical solutions

Several cross-checks of the model have been done by comparing calculations with known analytical solutions. The first case described here is stationary limit with no bulk recombination. Here I also neglect initial recombination. Equation for stationary ion density is:

$$\frac{\partial}{\partial z}\left(v_i \cdot n_i\right) = -J \tag{13}$$

that can be easily integrated (*E(z)* is negative) with boundary condition $n_i(a)=0$:

$$\mu_i \cdot E(z) \cdot n_i(z) = -J \cdot (a - z) \tag{14}$$

Together with (11) it gives equation for *E(z)*:

$$\frac{\partial}{\partial z}\left(E(z)^2\right) = -\frac{8 \cdot \pi \cdot q \cdot J}{\varepsilon \cdot \mu_i} \cdot (a - z) \tag{15}$$

And after integration

$$E(z) = \left(\frac{4 \cdot \pi \cdot q \cdot J}{\varepsilon \cdot \mu_i}\right)^{1/2} \left[b^2 + (a - z)^2\right]^{1/2} \tag{16}$$

Constant *b* can be found from (3). For zero HV impedance the anode voltage *V(a)* is equal to the supply voltage V_b and voltage drop across gap is

$$V_b = \left(\frac{4 \cdot \pi \cdot q \cdot J}{\varepsilon \cdot \mu_i}\right)^{1/2} \cdot b^2 \cdot \int_0^{a/b} (1 + y^2)^{1/2} \cdot dy \tag{17}$$

From where the following equation to determine the constant *b* is derived:

$$a \cdot \sqrt{b^2 + a^2} + b^2 \cdot \ln\left[\frac{a + \sqrt{b^2 + a^2}}{b}\right] = 2 \cdot V_b \cdot \left(\frac{\varepsilon \cdot \mu_i}{4 \cdot \pi \cdot q \cdot J}\right)^{1/2} \tag{18}$$

Here I assume that solution of eq. (18) exists. This is true if V_b is high enough or ionization rate is low. If this is not true, the formal solution of (13), (15) does not exist that means no stationary limit exist in asymptotic. Physically it happens because *E(a)* becomes zero and therefore there is no drift in the anode area. If there is no drift, space charge will increase with time permanently without converging to a stationary limit. In this case the limit is defined by recombination, which is neglected in this example.

As soon as *b* is known, *E(z)* and $n_i(z)$ can be defined with (16) and (18). Fig. 6 shows calculations and model computations (parameters *R* and *Z* are fixed to some very low values) for a set of ionization rates *J*, corresponding to different values of energy deposition E_v quoted in Fig. 6. There is a

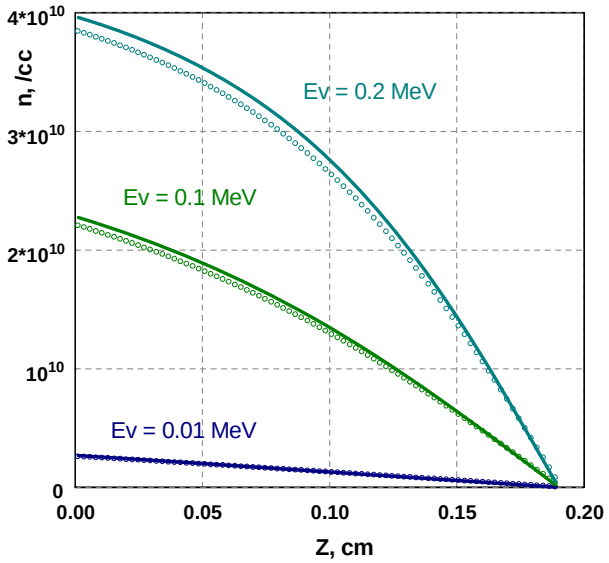

***Figure 6**: Ion density in gap calculated analytically (lines) and numerically (points) for three values of energy deposition in LAr.*

difference of not more than 3% between model and exact analytical result. This difference is due to the recombination rate is low but not zero in the model computations.

Another simple case when analytical solution exists is the case of no recombination, very low space charge density, and no impedance in the bias line. Thus, electric field and therefore drift velocities are constant in time and space and eqs. (1) are reduced to

$$\frac{\partial n_e}{\partial t} = J - v_e \cdot \frac{\partial n_e}{\partial z}; \qquad \frac{\partial n_i}{\partial t} = J + v_i \cdot \frac{\partial n_i}{\partial z} \tag{19}$$

which are equations of linear motion with obvious solution:

$$n_i(t,z) = \begin{cases} J \cdot t & \text{for} \quad 0 < z < a \cdot (1 - \frac{t}{\tau_i}) \\ J \cdot \tau_i \cdot \frac{a - z}{a} & \text{for} \quad a \cdot (1 - \frac{t}{\tau_i}) < z < a \end{cases} \tag{20}$$

and similar expression for electrons. These conditions can be reproduced in the model by lowing down recombination constant *R* and impedance *Z*. In order to avoid space charge effects, the energy deposition *J* must be sufficiently low. Fig. 7 shows function (20) calculated for three values of *t* and model computations for the case when *R*, *Z*, and *J* were reduced by factor of 100 with respect to their nominal values. As seen from the right plot, the space charge is not completely removed, so some difference between calculated and computed distributions can be observed (left plot). Nevertheless, the model can reproduce the main features of (20).

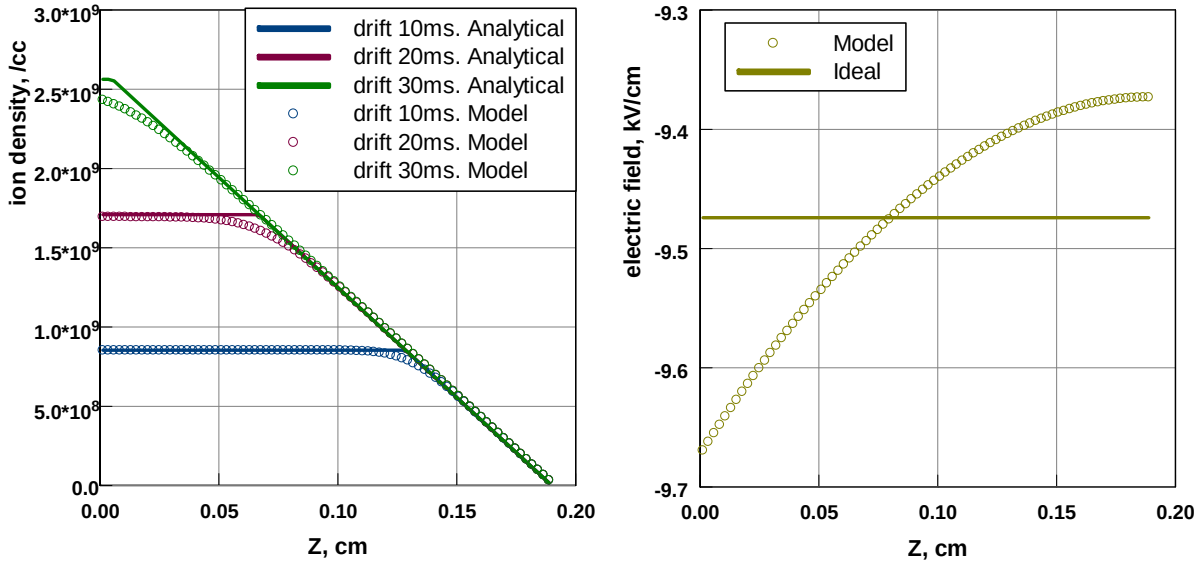

***Figure 7**: Model and analytical calculations of space charge distribution (left) and electric field in the gap (right).*

From (20) the average over gap can be calculated directly as:

$$n_{ia}(t) = J \cdot t \cdot \left(1 - \frac{t}{2 \cdot \tau_i}\right) \qquad \text{for} \quad 0 < t < \tau_i \tag{21}$$

and the same expression for electrons with replacing ion drift time τ_i by electron drift time τ_e. Also, by using densities (20), the bias current (4) can be calculated. It consists of two parts – electron and ion, the later one is:

$$I_i(t) = J \cdot q \cdot S \cdot a \cdot \frac{t}{\tau_i} \cdot \left(1 - \frac{t}{2 \cdot \tau_i}\right) \qquad \text{for} \quad 0 < t < \tau_i \tag{22}$$

Expression for electron part is exactly the same with proper drift time. Fig. 8 demonstrates how the model reproduces functions (21) and (22).

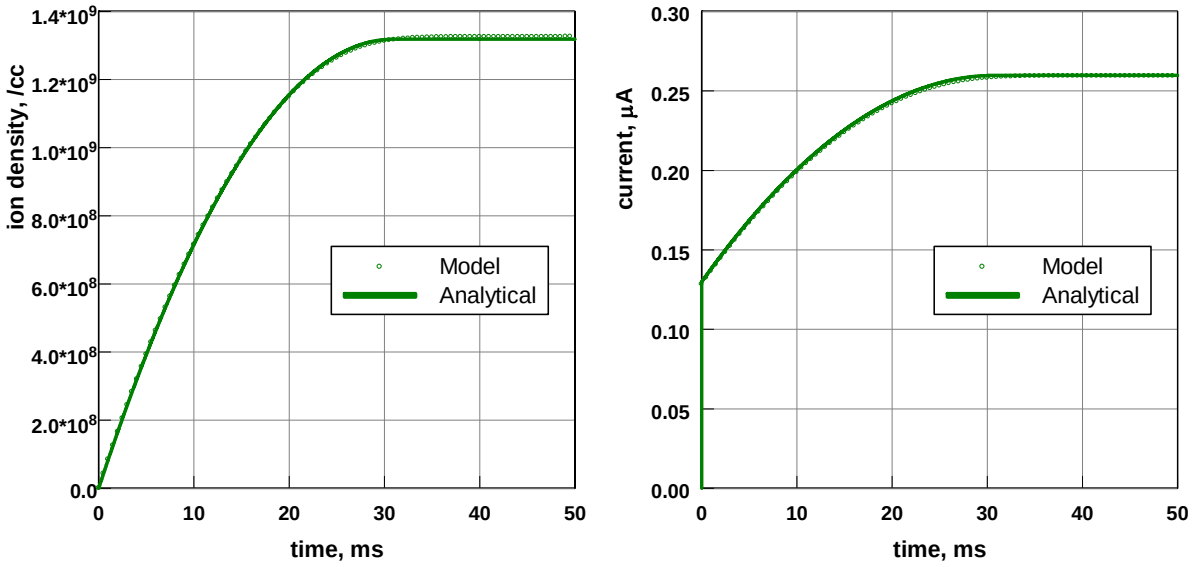

***Figure 8**: Model and analytical calculations of ion density (left) and bias current (right).*

The last case described here is the case of very low electric field. In this case both electron and ion drift can be neglected that reduces (1) to

$$\begin{aligned} \frac{\partial n_e}{\partial t} &= J - R \cdot n_e \cdot n_i \\ \frac{\partial n_i}{\partial t} &= J - R \cdot n_e \cdot n_i \end{aligned} \tag{23}$$

Both n_e and n_i are defined by the same equation with the same initial condition $n(0)=0$, that means $n_i(t)=n_e(t)$. So, (23) gives for ions (the same for electrons)

$$\frac{\partial n_i}{\partial t} = J - R \cdot n_i^2 \tag{24}$$

with solution

$$n_i(t) = n_R \cdot th(t / \tau_R); \qquad n_R = \sqrt{J/R} \quad \text{and} \quad \tau_R = 1/\sqrt{J \cdot R} \tag{25}$$

The model computations of this case is done by changing ν_m parameter in (6) to extremely low value that makes electron drift time much longer than the recombination time constant τ_R (~30μs for nominal J and R). Approximation of fast electrons is not valid in this case and computations

were done by original model with 1-*ns* time step. The result is shown in Fig. 9 together with function (25).

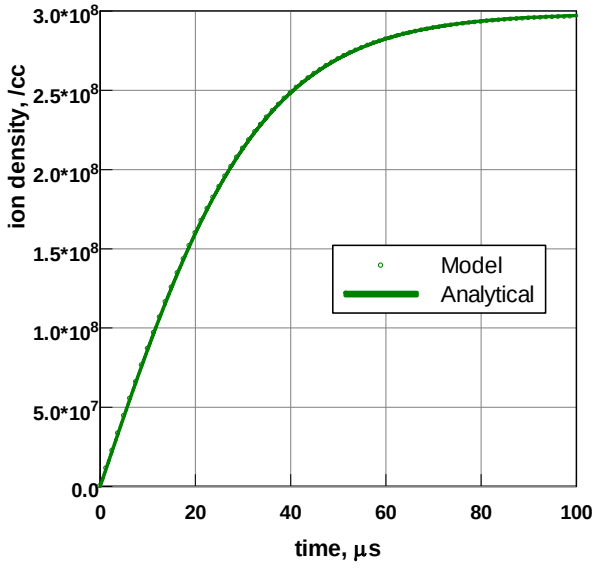

***Figure 9**: Model and analytical calculations of ion density at low electric field (the case of pure recombination).*

6. Numerical computations

In this chapter I summarize some results of computations performed to study how various parameters affect the gap space charge. Since recombination rate constant *R* of LAr is not well known, it is interesting to evaluate its contribution to the built-up space charge. Computations have been performed for a wide range of *R* from nearly zero to twice the nominal value. All other parameters are at their nominal values. Fig. 10 shows the ion density in the gap as a function of time. It is seen that for the lowest value of *R* the space charge density is twice higher than that for the nominal *R* value. The space charge distribution in gap is different for different *R* values that can be seen in the left plot of Fig. 10. This profile defines the ionization signal shape and therefore, the exact value of R must be known for calculations of induced signal.

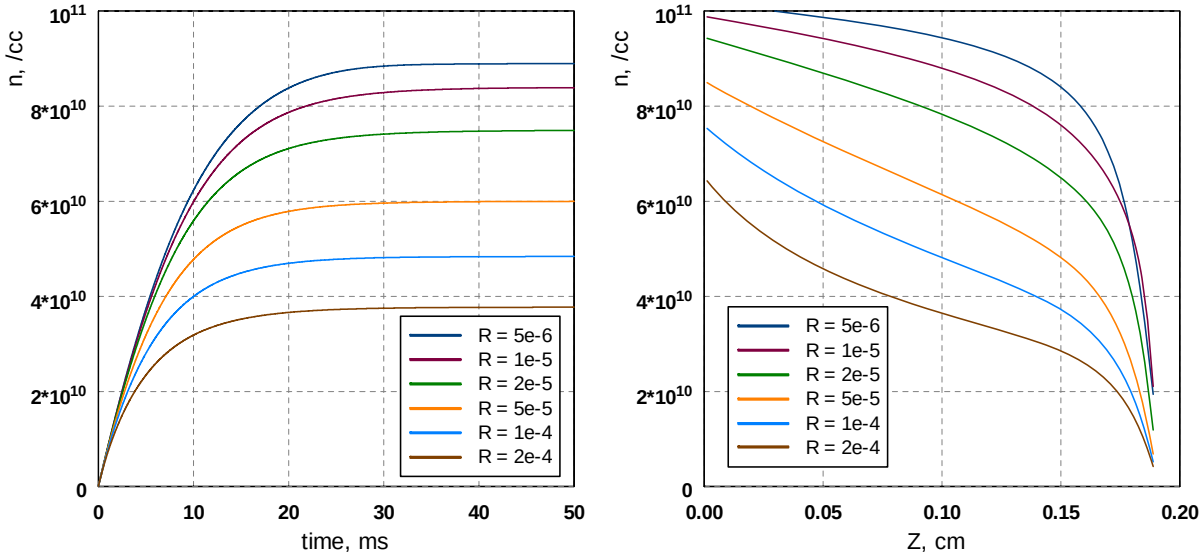

***Figure 10**: Build-up of ion density in the gap for different values of recombination rate constant.*

Fig. 11 shows stationary limit of ion density and anode current for different *R* values. There is a difference of factor ~2 between current at nominal recombination rate and in the case of zero recombination. This is another reason why it is important to know exact *R* value, especially in the case of higher impedance in the bias network, when voltage drop is high. It can be concluded that recombination process is not negligible at sLHC conditions and exact value of its rate constant must be known to make this model able to predict the detector performance.

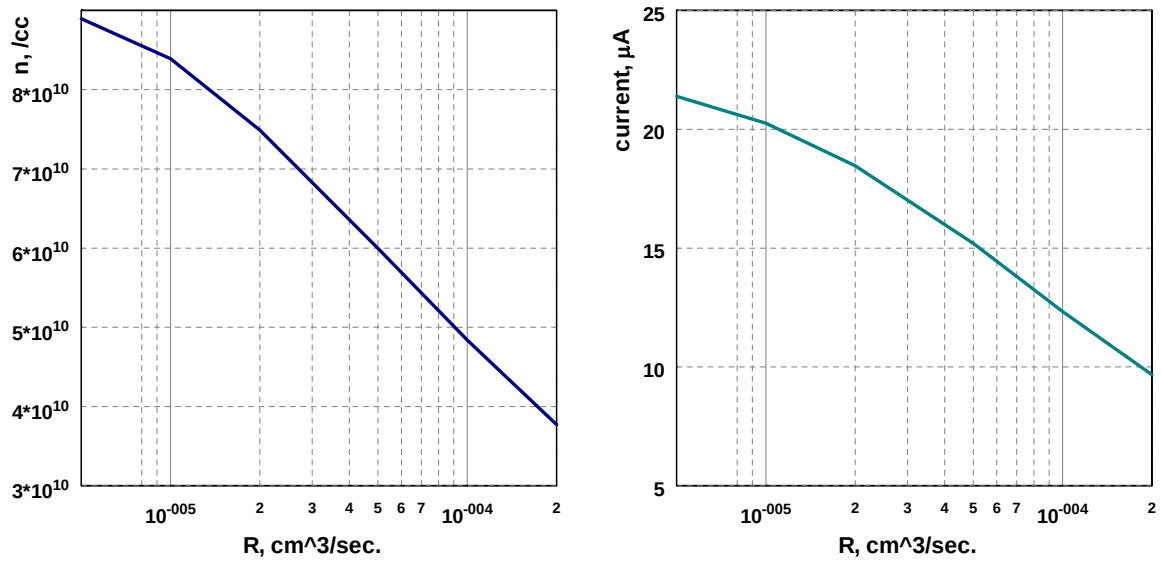

***Figure 11**: Space charge and current in HV line in stationary limit vs. recombination rate constant.*

Ion mobility is another important parameter which defines dynamics and asymptotic value of space charge. Computations have been performed for a wide range of ion mobility μ_i with other parameters fixed to their nominal values. Fig. 12 shows build-up of ions and their distribution in the gap for five different values of ion mobility. For lower mobility the longer time is needed to reach the stationary limit and more space charge is left in the gap.

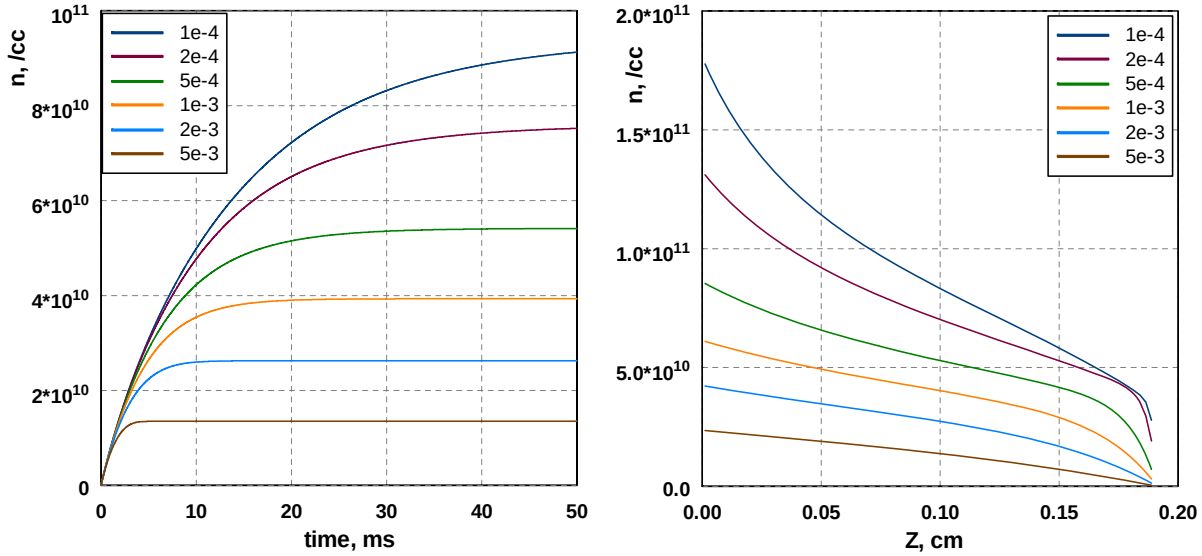

***Figure 12**: Ion build-up (left) and stationary distribution in gap for different mobility values (right).*

Dependence of space charge and current in HV line on the ion mobility is shown in Fig. 13. It can be seen that present uncertainty in the knowledge of mobility value leads to a variation of factor of two in the predicted value of ions density and anode current. Much better knowledge of actual ion mobility value is needed for reliable predictions of the detector performance.

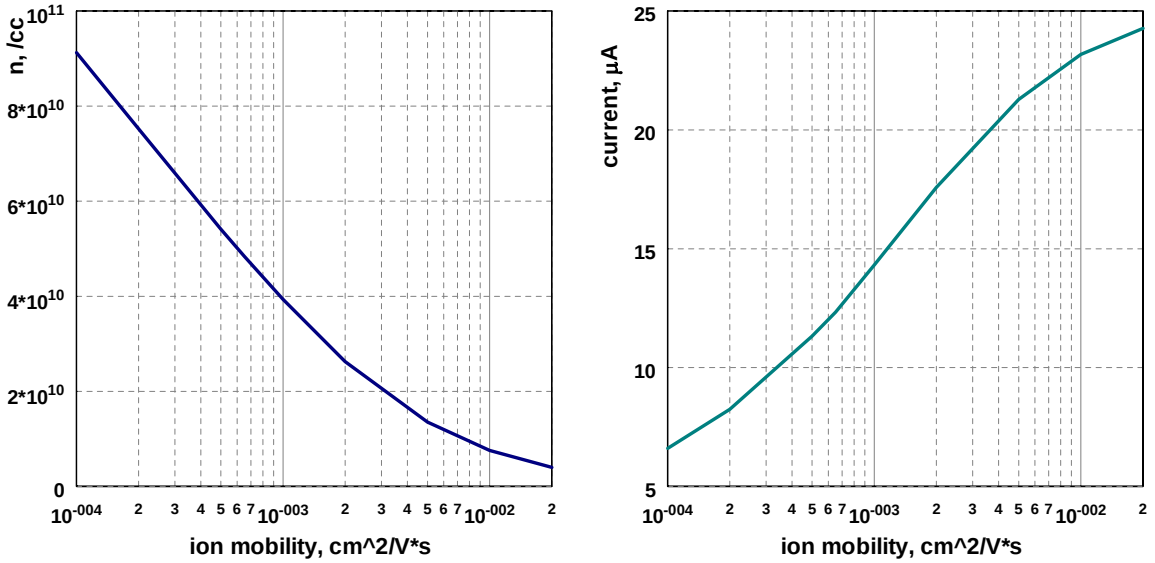

***Figure 13**: Space charge and current in HV line in stationary limit vs. ion mobility.*

The HV line impedance consists of two parts: resistors in distribution network and surface resistivity of kapton layers. The later have a variation of more than an order of magnitude in HEC segments; its actual value can be obtained from HEC construction data base. To check the effect of this resistivity, I've made calculations of space charge for a range of *Z* values. The result is shown in Fig. 14 and 15. All other parameters are at their nominal values.

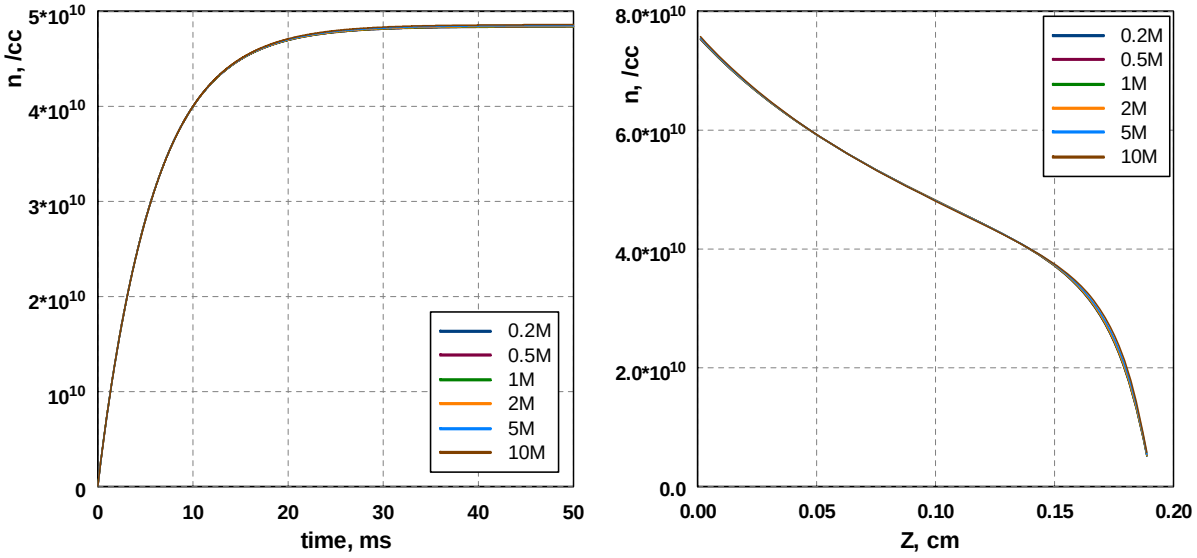

***Figure 14**: Ion build-up (left) and their stationary distribution in the gap for different values of impedance in HV line.*

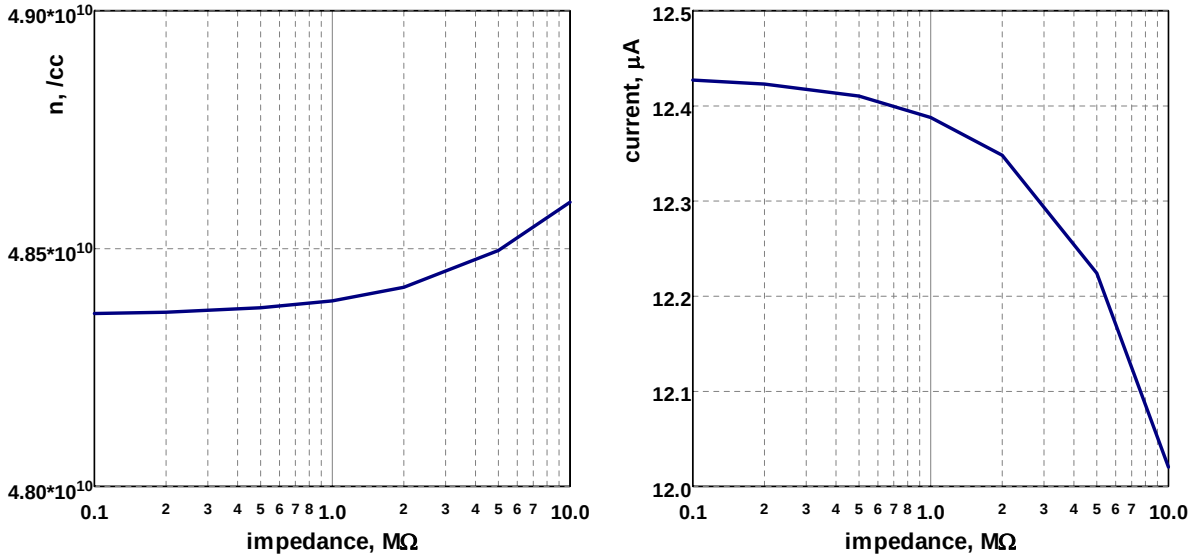

Figure 15*: Space charge and current in HV line in stationary limit vs. bias network impedance.*

It can be seen that HV drop does not affect much either ion build-up or ion distribution in the gap. This is because the higher impedance causes higher voltage drop, i.e. lower anode voltage. With lower field the ion (and electron) drift is slower that increases the ion density. At the same time longer drift causes more recombinations, that reduces the ion density. If the impedance is not very high, these two effects compensate each other; however in the case of actual HEC detector the effect could be significant because one HV line serves many gaps of large area.

7. Summary

The implementation of numerical calculations of charge build-up in LAr gap is mathematically very simple. It does not require any sophisticated algorithms or special libraries. The detail calculation of space charge dynamics (with very short time step of the order of 1 *ns*) is time consuming but for studies of high-rate effects it is not needed. Since electron drift is much faster than that of ion, the electron space charge can be neglected. In addition, actual time structure of ionization (periodical bunches) can be replaced by a uniform function for both cases of LHC and Protvino beam. In this case the time step can be increased up to ~10 μs that makes computations ~3000 times faster.

The present knowledge of ion drift mobility and electron-ion recombination rate constant is poor. It makes any calculation of high-rate effects in LAr unuseful and predictions unreliable, unless these two parameters are properly adjusted. Such adjustment can be (hopefully) done with data of Protvino tests. Otherwise a set of special measurements will be required.

References

1. John P. Rutherfoord, *Signal degradation due to charge buildup in noble liquid ionization calorimeters*, NIM A482 (2002) p.156

2. ATLAS-HEC Collaboration, *Performance of the ATLAS hadronic end-cap calorimeter in beam tests*, NIM A482 (2002) p.94

3. J. Thomas, D.A. Imel, *Recombination of electron-ion pairs in liquid argon and liquid xenon*, Phys. Rev. A36 p.614 (1987)

4. Bob. L. Henson, *Mobility of positive ions in liquefied argon and nitrogen*, Phys. Rev. 135 4A p.A1002 (1964)

5. K. Shinsaka, M. Codama, T. Srihanratana, et. al., *Electron-ion recombination rate constants in gaseous, liquid, and solid argon*, J. Chem. Phys. 88 (12) p. 7529 (1988)

Appendix

Table below contains a set of parameters and constants used in this Note as nominal values.

Parameter	Notation	Dimension	Value
Gap width	a	cm	0.19
Pad area	S	cm^2	100
LAr dielectric constant	ε		1.5
Bias voltage	V_b	V	1800
Electric field	E	kV/cm	9.474
HV line impedance	Z	MΩ	1
HV line time constant	τ	ms	1
Energy deposition per BC	E_v	MeV	1
Bunch crossing time	τ_b	ms	1
LAr ionization yield	W_i	eV	23.6
Thomas-Imel field	E_T	kV/cm	0.84
Escape factor	r		0.958
Ionization rate	J	cm^{-3}/s	$8.546 \cdot 10^{12}$
Steady bias current	I	μA	25.98
Recombination rate	R	cm^3/s	10^{-4}
Recombination stationary density	n_R	cm^{-3}	$2.99 \cdot 10^8$
Recombination time constant	τ_R	μs	33.5
Ion mobility	μ_i	$cm^2/V \cdot s$	$6.5 \cdot 10^{-4}$
Ion drift velocity	v_i	cm/s	6.158
Ion drift time	τ_i	ms	30.85
Electron saturation velocity	v_m	mm/μs	13.4
Electron drift velocity	v_e	mm/μs	4.433
Electron drift time	τ_e	ns	429